ADVANCED INTELLIGENT SYSTEMS
Open Access
www.advintellsyst.com

Design and Scalable Fast Fabrication of Biaxial Fabric Pouch Motors for Soft Robotic Artificial Muscle Applications

*Ayse Feyza Yilmaz, Kadir Ozlem, Mehmet Fatih Celebi, Bahman Taherkhani, Fatma Kalaoglu, Aslı Tunçay Atalay, Gokhan Ince, and Ozgur Atalay**

Soft pouch motors, engineered to mimic the natural movements of skeletal muscles, play a crucial role in advancing robotics and exoskeleton development. However, the fabrication techniques often involve multistage processes; they lack soft sensing capabilities and are sensitive to cutting and damage. This work introduces a new textile-based pouch motors with the capacity for biaxial actuation and capacitive sensory functions, achieved through the application of computerized knitting technology using ultrahigh molecular weight polyethylene yarn (Spectra) and conductive silver yarns. This method enables the rapid and scalable mass fabrication of robust pouch motors. The resulting pouch motors exhibit maximum lifting capacity of 10 kg, maximum contraction of 53.3% along the *y*-axis, and transverse extension of 41.18% along the *x*-axis at 50 kPa pressure. Finite element analysis closely matches the experimental data. The capacitance signals in relation to contraction motion are well suited for detecting air pressure levels and hold promise for applications requiring robotic control. Notably, it effectively elevates an ankle joint simulator at a 20° angle, highlighting its potential for applications such assisting individuals with foot drop. This study presents a practical demonstration of the soft ankle exosuit designed to provide lifting support for individuals facing this mobility challenge.

1. Introduction

The skeletal muscles within the human body act as dynamic power sources,[1] enabling a wide array of movements, from common everyday actions like gripping a glass to the physically demanding activities of walking and engaging in sports.[2,3] However, these muscles can lose their functionality due to injuries, traumas, or specific neuromuscular disorders, resulting in numerous challenges for affected individuals in their daily lives.[4,5] In response to these challenges, soft robotic systems have been developed to assist individuals in regaining their independence and improving their quality of life.[6–11] These systems, employing soft pouch motor structures, show significant promise in providing assistance to individuals with impaired muscle function by mimicking muscle-like contraction movements.[12–16] Nevertheless, the development of scalable and mass-producible soft pouch motors with integrated sensing capabilities is one of the ongoing challenges in the realm of soft robotics. The automation of robot fabrication, spanning design to assembly, is crucial to reducing prototyping costs and enhancing scalability for mass production. Moreover, the development of cost-effective, efficient, and high-quality mass production methods is imperative to meet the increasing demand for soft pouch motors. It is also important to highlight those novel approaches, like incorporating sensors directly into the framework of motors or devising external sensing systems to enhance these functionalities of motors, have received limited exploration. Additionally, the adoption of more robust materials is needed to enhance the durability and reliability of these motors, particularly in demanding applications.

A. F. Yilmaz, B. Taherkhani, F. Kalaoglu, A. T. Atalay, O. Atalay
Faculty of Textile Technologies and Design
Textile Engineering Department
Istanbul Technical University
Istanbul 34437, Turkey
E-mail: atalayoz@itu.edu.tr

The ORCID identification number(s) for the author(s) of this article can be found under https://doi.org/10.1002/aisy.202300888.

DOI: 10.1002/aisy.202300888

K. Ozlem, G. Ince
Faculty of Computer and Informatics Engineering
Computer Engineering Department
Istanbul Technical University
Istanbul 34469, Turkey

M. F. Celebi
Faculty of Technology
Mechatronics Engineering Department
Marmara University
Istanbul 34854, Turkey

The process of muscle contraction is a biological phenomenon that depends on the reduction in muscle length, enabling it to produce movement and generate force.[17,18] The force generated by muscles exceeds the opposing force, such as the weight being lifted, resulting in joint movement.[19–21] Soft pouch motors have emerged as a specialized class of actuators that have garnered considerable attention due to their remarkable ability to mimic this complex motion and functionality observed in natural muscles. These motors have flexible and soft structures, setting them apart from conventional rigid motors, and their softness allows for safe interactions with the environment.[22,23] This type of actuator is fabricated using flexible materials, which exhibit contractile and expansile properties when exposed to various external stimuli, including fluidic pressure,[24] electrical stimulation,[25] thermal variations,[26] and chemical reactions.[27] One of the standout features of soft pouch motors is their high power-to-weight ratio, making them exceptionally suitable for applications requiring lifting and the generation of substantial force. The combination of high-power output and low-weight properties enables these actuators to efficiently and effectively perform lifting tasks. These unique characteristics enable soft pouch motors to deliver precise and adaptive actuation responses to various conditions and requirements, making them highly suitable for a wide range of applications involving soft artificial muscles, from medical devices to robotic systems and from micromechanical mechanisms to automotive applications.[16,27]

The fundamental principle behind the contraction motion in soft pouch motors lies in the controlled deformation of their constituent material or structures themselves. The specific mechanisms used to accomplish contraction vary depending on the design of the motor and the actuation concept. In numerous cases, these actuators achieve contraction through the physical shortening of their structural length. Traditionally, these motors have been recognized for their uniaxial contraction along the y-axis when pressurized fluid is introduced into the motor, causing the material to contract.[13,28,29] These actuators radially expand in response to changes in gas pressure. The introduction of pressurized air or gas induces the contraction of the flexible material, resulting in a reduction in length and subsequent contraction motion.[30] While many soft pouch motors predominantly exhibit unidirectional motion along the y-axis, integrating capabilities for movement along both the x and y axes can introduce new concepts.

The effectiveness and capabilities of soft pouch motors depend heavily on the base materials used in their fabrication. Soft pouch motor fabrication commonly relies on materials like film[13,14,28] and textiles.[22,26,31] Film materials possess inherent flexibility, which compromises their mechanical durability. This makes them more prone to deformation or tearing with prolonged or intense usage. Moreover, while polymer film materials offer flexibility, they may not meet the necessary level of comfort required for wearable devices. Comfort and flexibility are crucial for extended wear, and polymer film actuators may fall short of meeting these criteria. Their sharp edges can cause discomfort or irritation when in contact with the body. Furthermore, the aesthetic suitability and compatibility of polymer film actuators with wearable devices may be limited. Design and style are essential for the acceptance of wearable technology, and these actuators may not align with user preferences. Considering these factors, polymer film actuators are generally not the preferred choice for wearable technology applications. Alternative materials, such as textiles, offer superior comfort, flexibility, and integration capabilities, making them more suitable for wearable device design.

In contrast, textile-based materials offer significant advantages for pouch motors, especially in wearable applications prioritizing flexibility and comfort. Textile actuators integrate into garments, enabling aesthetically pleasing designs. They can be directly embedded into textiles, facilitating the development of smart clothing with integrated sensing and actuation capabilities. Moreover, textile actuators are washable, simplifying maintenance—a critical feature for wearable devices in close contact with the body. Textiles boast several other benefits, including being lightweight, conformal, and resilient against repeated stresses and abrasions encountered during regular use. Unlike flexible polymer films, textiles can withstand wear and tear, ensuring prolonged performance. With their hierarchical structure—from fibers to yarns, and further to fabrics—textiles provide a versatile platform for actuator development. Actuators are engineered at various levels within this hierarchical structure to suit specific functionalities, utilizing appropriate fabrication methods accordingly. For example, at the yarn level, techniques like melt spinning, wet spinning, and electrospinning are employed, while at the fabric level, methods such as weaving, knitting, or braiding fabrication are utilized.[32] Instead of these technologies, actuators can be produced using cutting, sewing, and bonding methods with commercial woven and knit fabrics.[33–42] The fabric-based actuator literature predominantly focuses on actuators constructed from commercially available thermoplastic polyurethane (TPU)-coated woven fabrics via laser cutting and thermal bonding fabrication methods, and these actuators often lack embedded sensors (**Table 1** and Table S1, Supporting Information). Woven fabrics, compared to knitted fabrics, are less flexible, restricting the motion range of pouch motors and hindering their ability to perform complex movements.[31] Furthermore, the fabrication process for woven pouch motors is less rapid for mass production. This results in increased production time and costs, while joining woven materials can pose challenges, especially on a larger scale, necessitating additional methods or equipment for material fusion and complicating the manufacturing process. The response to this challenge lies in computerized knitting fabrication. However, current studies indicate that actuators designed and fabricated using computerized knitting machines feature a tubular design, often lacking soft sensing capabilities, and exhibiting sensitivity to cutting and damage. They primarily concentrate on bending and coiling motions. These textile fabric actuators have been summarized in Table 1.

In this article, we present the design and characterization of a novel biaxial soft knitted sensing pouch motor for foot drop, inspired by the contraction behavior of the human muscle (**Figure 1**a,b). This study investigates the potential of utilizing textile computerized knitting technology using high-performance Spectra yarn to make it with a cut-resistant feature for the development of soft pouch motors with embedded sensing capability (Figure 1c). Knitting technology provides a seamless, fast, scalable, and mass-production fabrication approach, instead of relying on the assembly of individual parts. The ability of the pouch motor to perform contraction motion, driven by

Table 1. Overview of reported textile fabric actuators.

References	Material	Fabrication method	Actuation	Sensing	Motion	Comment
[26]	TPU-coated woven fabric	Laser cutting and heat bonding	Joule heating	Capacitive sensor (not embed)	Contraction	The sensor is integrated with heat bonding to the actuator
[69]	Woven fabric	Heat bonding	Pneumatic	–	Contraction	–
[70]	TPU-coated woven fabric	Laser cutting, thermal bonding	Pneumatic	–	Contraction	Contraction motion is for compression
[71]	TPU-coated woven fabric	Thermal bonding	Pneumatic	–	Contraction	–
[72]	TPU-coated woven fabric	Thermal bonding	Pneumatic	Pressure sensor and displacement sensor (not embed)	Contraction	Sensors are rigid and commercially available. 3D printing and bonding fabrication methods are used to integrate of sensor into the actuator
[44]	Lycra yarn, polyamide yarn, melting yarn	Computerized knitting	Pneumatic	–	Bending	Tubular structure
[73]	The boucle of fancy yarns with the core of PU filament and the sheath of twisted PET fibers	Computerized knitting	Pneumatic	–	Bending, coiling.	Tubular structure
[74]	Acrylic yarn, elastic yarn, conductive yarn	Computerized knitting	Pneumatic	Resistive pressure sensing, swept frequency capacitive sensing (embedding sensor)	Bending	Tubular structure
[75]	Acrylic yarn, shrinking yarn, elastomeric yarn, conductive yarn	Computerized knitting	Pneumatic	Resistive sensing	Bending, coiling.	Tubular structure. Only, bending actuator consists of resistive sensing

radial expansion and transversal extension, has been thoroughly examined. Addressing the need for improved sensing capabilities and scalable mass production methods is crucial to unlocking the potential of soft pouch motors. It will not only expand their utility but also drive innovation in areas where their unique characteristics can make a difference.

2. Design Concept and Fabrication of Knitted Sensing Pouch Motors

In this study, a novel high-performance pouch motors design with sensing capabilities was achieved by seamlessly integrating technical and electrically conductive yarns using computerized weft knitting technology (Movie S1, Supporting Information). The classification of our pouch motor as "high performance" originates from the technical properties of Spectra yarn, which are not typically found in other traditional textile yarns. In the fabrication of soft pouch motors using knitting techniques, Spectra yarn serves as the base material, enabling the transfer of high-performance attributes such as cut resistance and strength to the pouch motor.

The knitted pouch motor design is shown in **Figure 2**a. Figure S1, Supporting Information, shows the dimensions and knitted design simulation image of the pouch motor. The design of the knitted pouch motor is universally applicable, facilitated by the utilization of computerized knitting technology. The dimensions of the pouch motor have been optimized considering the foot width, foot and ankle attachment points, as it will be used for foot drop syndrome application. Based on foot width measurements from 10 adult women and men, the actuator width was selected as 9 cm (Figure S2 and Table S2, Supporting Information). The average foot width for women is 9 cm, while for men, it is 10 cm. A 10 cm-wide pouch motor actuator aesthetically appears too broad and protruding for the foot width of women, hence a 9 cm width was chosen. This width also accommodates men's feet adequately. The actuator length is set at 19 cm, chosen as the optimum length required for secure attachment to the foot and ankle (Figure S3, Supporting Information). Attachment areas for the foot and ankle are set at 4 cm to ensure secure fastening.

In the construction of the pouch motors, three different types of textile yarns have been utilized: Spectra, conductive, and elastomeric yarns. These yarns play crucial roles in ensuring the functionality and performance of the motors, with each contributing distinct mechanical, electrical, and elastic properties to the overall design. The results of the tensile strength tests for these yarns are presented in Figure 2a(i). The high tensile strength exhibited by Spectra yarns, as evidenced by their minimal deformation under load, highlights their exceptional durability and suitability for applications requiring robust mechanical performance. Conductive threads, on the other hand, demonstrate a balance between strength and flexibility, making them well suited for use in electrical connections within the pouch motor. Their ability to maintain structural integrity while accommodating various mechanical stresses is essential for reliable electrical

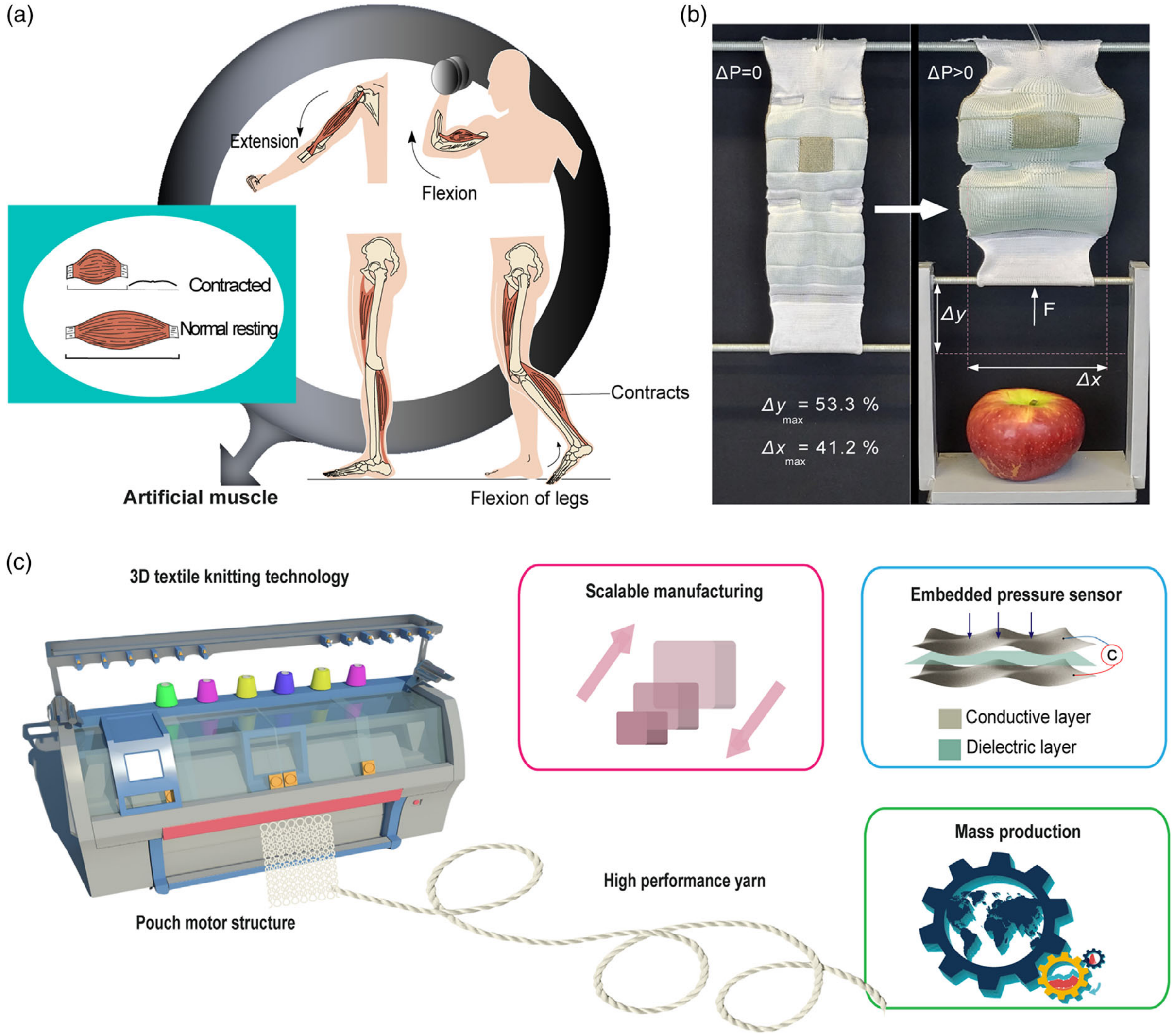

Figure 1. The design concept of a soft biaxial sensing pouch motors. a) Illustration of artificial muscles bioinspiration from human muscles. b) Prototype of the textile knit-based pouch motors. Δy represents the linear contraction along the y-axis; Δx indicates the transversal extension. c) The sensing pouch motors are produced using 3D computerized knitting technology, featuring scalable mass production, high-performance yarn, and embedded pressure sensors.

connectivity. Elastomeric yarns exhibit notable flexibility, as indicated by their ability to undergo significant deformation and recover to their original state. This property is crucial for applications where the pouch motor needs to adapt to changing shapes and environments, such as in soft robotics. The tensile test results highlight the unique characteristics of these yarns and their contributions to pouch motor technology, emphasizing the importance of selecting the right yarn type for specific design requirements, as shown in Figure 2a(i).

The base yarn of the pouch motor, Spectra yarn, is known for its exceptional strength, particularly its high tensile strength. This property makes it suitable for applications where the pouch motor needs to withstand significant loads. It has minimal stretch compared to other fibers, which is beneficial for maintaining the desired shape of the pouch motor. It is lightweight and advantageous in weight-sensitive applications such as wearable devices or soft artificial muscle robotics. It is highly resistant to chemicals, making it suitable for use in environments where exposure to corrosive substances may occur. Spectra yarn also boasts good abrasion resistance, contributing to the durability of the pouch motor. Additionally, its UV resistance makes it suitable for outdoor applications.[43] This yarn offers flexibility while maintaining strength, crucial for achieving desired movements in soft robotics. These properties make Spectra yarn a suitable choice for the development of soft textile pouch motors using weft knitting technology. To impart a recovery feature to the pouch motor, elastomeric yarn is intermittently incorporated. When inflated and deflated, the pouch motor demonstrates the ability to self-recover even after extended cycles. The combination of Spectra yarn and elastomeric yarn empowers the pouch motor with exceptional recovery capabilities. After undergoing numerous inflation and deflation cycles, the motor

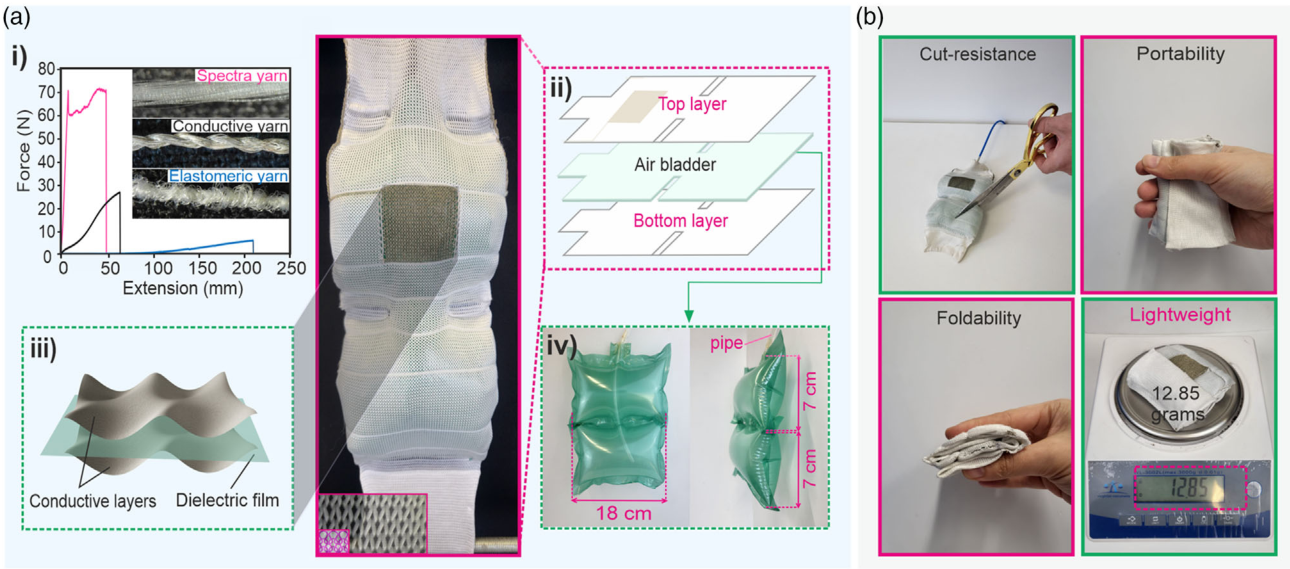

Figure 2. a) Knitted sensing pouch motors. i) The yarns used in the knitting design of the sensing pouch motors: ultrahigh molecular weight polyethylene yarn, conductive yarn, and elastomer yarn. ii) Structure of the pouch motor. iii) Capacitive sensor structure of pouch motors. iv) The design and dimensions of the air bladder placed inside the pouch motors. b) Demonstration of the cut resistance, portability, foldability, and lightweight features of pouch motors.

consistently reverts to its original shape and dimensions. This feature ensures long-term reliability and durability in applications requiring repeated use. Electrically conductive silver-coated yarn is used in establishing and maintaining capacitive pressure sensor and electrical connections within the pouch motor. Conductive yarns enable the motor to transmit and receive capacitive signals effectively, making it responsive to pressure and contraction deformation.

The pouch motor is fabricated through the seamless integration of two layers consisting of upper and lower weft looped knitted fabrics, utilizing a digital knitting machine, as depicted in Figure 2a(ii). An air bladder is inserted between these layers to allow the pouch motor to inflate.

The main benefits of knitting fabrication technology are mass production and scalability.[44] In the process of fabricating a knitted pouch motor using a computerized knitting machine, the knit design is initially converted into a digital format compatible with the software of the machine. Then, the machine is programmed to knit pattern using yarns. The machine builds the structure of the pouch motor course by course as it knits, following preprogrammed instructions. The pouch motor is constructed with a knit structure in the form of a double-layered single jersey, while the contraction line is designed with a one-layered single jersey knit structure. The knitting process is executed by electronically controlled knit needles that move according to programmed instructions. These instructions dictate the movement of the needles along with the yarns to create the pouch motor design. The machine operates by feeding yarns through the needles and manipulating them to form loops on knitting needle bed (Movie S1, Supporting Information). As the needles move, they interlock the yarns to create pouch motor structure. Finally, the finished pouch motor is removed from the knitting machine.

The development of flexible and soft pressure sensors holds great significance, especially in the soft robotics. A variety of sensing technologies have been explored in prior works.[45–56] Among these, the capacitive sensing technology employing parallel plate structures has gained popularity due to its signal repeatability, insensitivity to temperature, and relative design simplicity, among other advantages.[57,58] Figure 2a(iii) illustrates the capacitive pressure sensing technology embedded within the pouch motor structure, consisting of conductive electrodes and a dielectric TPU film. The embedding sensor had dimensions of 3 cm in length by 3 cm in width, with a dielectric thickness of 38.1 μm. During the knitting fabrication process of the knitted pouch motor, the conductive yarns are knitted into the structure of the pouch motor using a technique called intarsia. Intarsia is a knitting method where different yarns are used to create distinct patterns or designs within the knitted fabric. This integration ensures that the electrodes are seamlessly embedded within the knitted structure of the pouch motor, allowing for efficient electrical conductivity and functionality. By stitching the lower conductive knitted layer and the dielectric layer into the upper conductive electrode, we ensured their secure placement inside the pouch motors. Using a thin thermoplastic film for the dielectric layer resulted in higher baseline capacitance, enhancing sensor robustness against parasitic capacitance in the readout circuitry.[59] Furthermore, the conductive connection points from the pressure sensor were embedded within the knitted surface of the electrodes, enabling flexibility, and secure connections for real-life applications. Embedding sensor is inherently more stable and less prone to movement or detachment compared to externally attached sensors. This ensures consistent and reliable data acquisition during operation of pouch motor. Our knitting embedding fabrication approach eliminates the need for additional adhesives or heat press processes, reducing the risk of failure points and enhancing the durability and longevity. Overall, while postintegration of sensors may provide some convenience, the benefits of embedded production, including enhanced stability, seamless integration, and improved durability, make it a more favorable choice for achieving reliable sensing capabilities in soft robotics.

The activation of the pouch motor through air pressure results in contraction, while the use of weft knitting technology imparts it with the ability to deform easily and extend in the course direction. This combination of features enhances the performance of the pouch motor, allowing for both transverse extension and increased contraction. To enable the transverse extension, it is necessary to incorporate an air bladder within the pouch motor with a width twice that of the motor itself (Figure 2a(iv)). This design choice is crucial in achieving optimal functionality.

The novel pouch motor developed in this study exhibits a set of features, making it a versatile and valuable component in the realm of soft artificial muscle applications (Figure 2b). The incorporation of Spectra yarn into the pouch motor design provides it with a cut-resistant feature (Movie S2, Supporting Information). Its compact and lightweight design makes the pouch motor highly portable, offering ease of transport and integration into various robotic systems. The flexible nature of the pouch motor allows for convenient folding, enabling efficient storage and deployment when needed. With its lightweight design, the pouch motor maintains ease of use, effectively reducing the overall weight of soft robotic applications.

3. Simulation Procedure

For the macroscale simulation, the knitted textile-based material properties were considered as anisotropic hyperelastic material.[31] Previous numerical studies for soft actuators have concentrated on isotropic hyperelastic materials.[60,61] However, there are some examples of textile-based soft actuator simulation in the literature review.[31,62] Some of the constitutive models that existed in ABAQUS software for anisotropic material modeling include the Holzapfel–Gasser–Ogden (HGO) and Fung models. The HGO strain energy formula is as follows:

$$U = C_{10}(\overline{I_1} - 3) + \frac{1}{D}\cdot\left(\frac{(J^{\mathrm{el}})^2 - 1}{2} - \ln J^{\mathrm{el}}\right) + \frac{k_1}{2k_2}\sum_{\alpha=1}^{N} e^{k_2}\overline{E}_\alpha^2 - 1 \tag{1}$$

$$\overline{E}_\alpha = \kappa\,(\overline{I_1} - 3) + (1 - 3\kappa)\,(\overline{I}_{\alpha\alpha} - 1) \tag{2}$$

where κ, k_1, k_2, D, and C_{10} are temperature-dependent material parameters that are imported into the Abaqus2021 software. N is the fibers families number ($N \leq 3$). I_1 is the first constant of the Cauchy–Green tensor. The material fitting tool permits to define boundary conditions, Poisson's ratio, initial parameters obtained from HGO model, and experimental equibiaxial data. Course and wale directions are corresponding to $(\sigma_{\theta\theta}, \sigma_{zz})$. A least-square method for the stress–strain functions in both directions was utilized as follows:

$$\chi = \sum_{i=1}^{n} \left[(\sigma_{\theta\theta} - \sigma_{\theta\theta}^{\mathrm{model}})_i^2 + (\sigma_{zz} - \sigma_{zz}^{\mathrm{model}})_i^2\right] \tag{3}$$

To design the presented pouch motor in Abaqus2021 software, two identical shell plates were used, which are placed at a distance of 0.5 mm from each other (**Figure 3**a(i)). To fit the boundary conditions appropriate to the experimental work, as shown in Figure 3a(ii), the surfaces under pressure were defined by partitioning, and the air pressure was uniformly applied to all internal regions of the pouch motor. The mesh used for this simulation, according to Figure 3a(iii), is C3D10M, and its number is 1421. The simulation of the front surface of the pouch motor is presented in Figure 3b and Movie S3, Supporting Information. The simulation image of the lateral side of the knitted pouch motor, illustrating radial expansion, is depicted in Figure 3c and is also available in Movie S3, Supporting Information. The experimental data and the simulation of knitted pouch motor both exhibited similar contraction behavior, as shown in Figure 3d. The simulation explains the experimental results with a 4% margin of error.

4. Results

4.1. Mechanical Characterization

We experimentally characterized the pouch motor by utilizing an air compressor for pneumatic actuation and a precision regulator for pressure adjustment. Upon inflation through the application of pressure, our pouch motor demonstrates features, including radial expansion and transverse extension, as illustrated in **Figure 4**a,b. The transverse extension deformation sets it apart from traditional pouch motors. The knitted pouch motor demonstrates both radial expansion and transversal extensions, leading to a contraction ratio of ≈53.3%. The behavior of up to 41.18% extension along the x-axis can be attributed to the structure of the knitted fabric, which allows the loops to expand laterally. Notably, with increasing pressure, we observe a corresponding increase in contraction, highlighting the sensitivity of our design to pneumatic changes. The pouch motor functions as a specialized mechanical artificial muscle actuator designed to exert forces for inducing motion in objects. Its primary function is to convert pneumatic power into pulling force, allowing it to exert forces and induce motion.

The theoretical contraction ratio for conventional pouch motors can be obtained using the following equations, assuming cylindrical surfaces and radial expansion:

$$L_0 = 2r\theta \tag{4}$$

$$r\sin\theta = \frac{L}{2} \tag{5}$$

where L_0 is the initial length of the pouch before deformation, r is a radius of the curve, L is the length of the inflated pouch, and θ is the central angle of the circular segment

$$A = 2r^2\theta - Lr\cos\theta \tag{6}$$

where A is the cross-sectional area of the pouch.

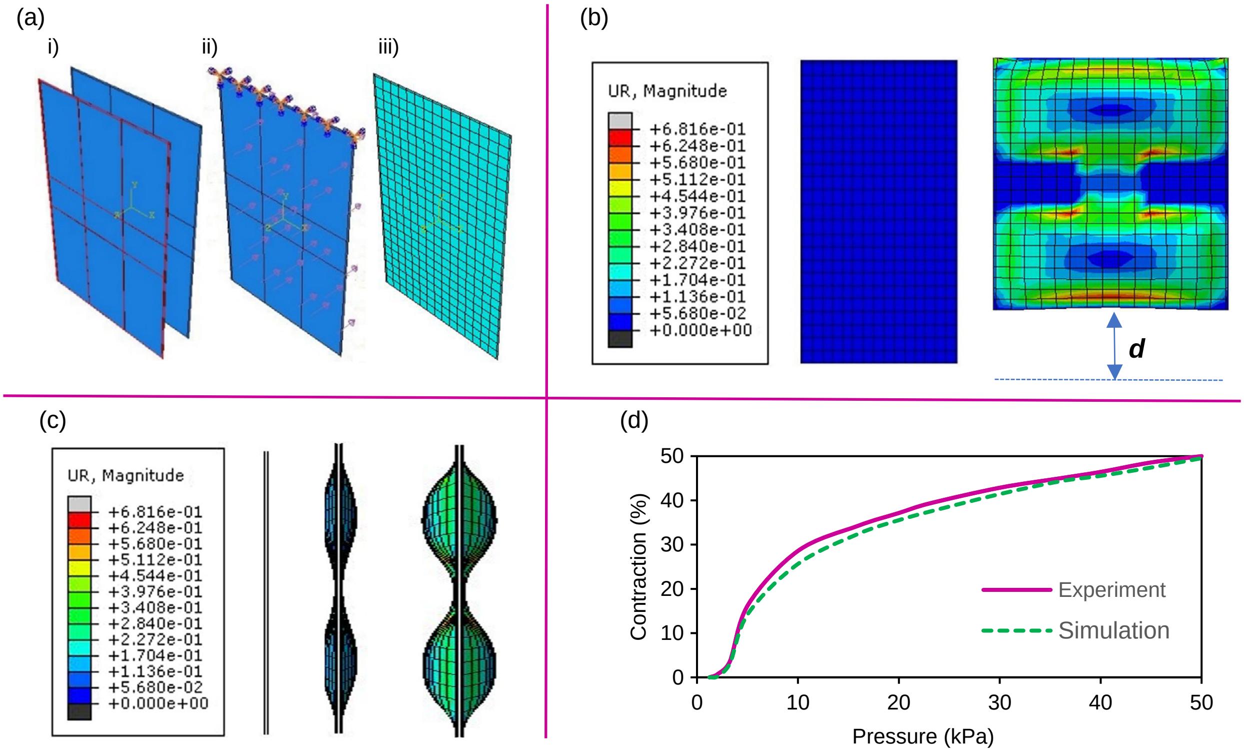

Figure 3. Simulation procedure of soft knitted pouch motor. a) i) Pouch motor structure with the distance of 0.5 mm between each surface, ii) boundary conditions, and iii) mesh of the pouch motor. b) Numerical images in the frontal view. c) Numerical images in the lateral view. d) Comparison of contraction behavior: simulation versus experimental results.

The volume of the pouch V can be derived as

$$V(\theta) = AD = \frac{L_0^2 D}{2}\left(\frac{\theta - \cos\theta\sin\theta}{\theta^2}\right) \tag{7}$$

where D is a width of the pouch. The length L can then be derived from the geometry as

$$L(\theta) = L_0\frac{\sin\theta}{\theta} \tag{8}$$

The energy conservation equation derived from the equilibrium between input work dW_{in} and dW_{out} output work is given by

$$-FdL = PdV \tag{9}$$

where F is the tension force, P is the inner pressure of the pouch, and dL and dV are the displacements in length and volume. The force as a function of the angle can then be derived as

$$F(\theta) = -P\frac{dV}{dL} = -P\frac{\frac{dV}{d\theta}}{\frac{dL}{d\theta}} = L_0 DP\frac{\cos\theta}{\theta} \tag{10}$$

L_e is defined as the ratio of total deformation to the initial length of the longitudinal edges L_0 as

$$L_e = \frac{L_0 - L}{L_0} = 1 - \frac{\sin\theta}{\theta} \tag{11}$$

The theoretical maximum contraction ratio of the linear traditional pouch motor is $L_e\ (\pi/2) = \frac{\pi - 2}{\pi} \approx 0.363$ (36.3%). However, pouch motors are not able to reach this theoretical value due to the force decreasing significantly in the later part of the contraction as the angle θ reaches 90° and the edges of the pouch not being able to deform in a circular shape. Thus, the practical maximum contraction ratio of the linear traditional pouch motors is closer to 30%.[16] However, it can vary depending on parameters such as design, material, and fabrication technique. Our pouch motor is noted as having a high strain due to surpassing the contraction ratio of traditional pouch motors. This is attributed to the inherent mechanical characteristics of knit structure, as depicted in Figure 4d. Knitting involves interlocking loops of yarn, which offer inherent flexibility, allowing for greater transverse extension compared to other manufacturing methods like weaving or braiding. In our study, we inserted an air bladder into the knitted pouch motor, twice as large as the pouch motor itself, enhancing the opening of the knitting loops and facilitating increased transverse extension. This combination of features enhances the performance of pouch motor, allowing for both transverse extension and increased contraction.

The knitted structure of the pouch motor, characterized by its course (the horizontal rows of loops) and wale directions (the vertical columns of loops), plays an important role in its actuation

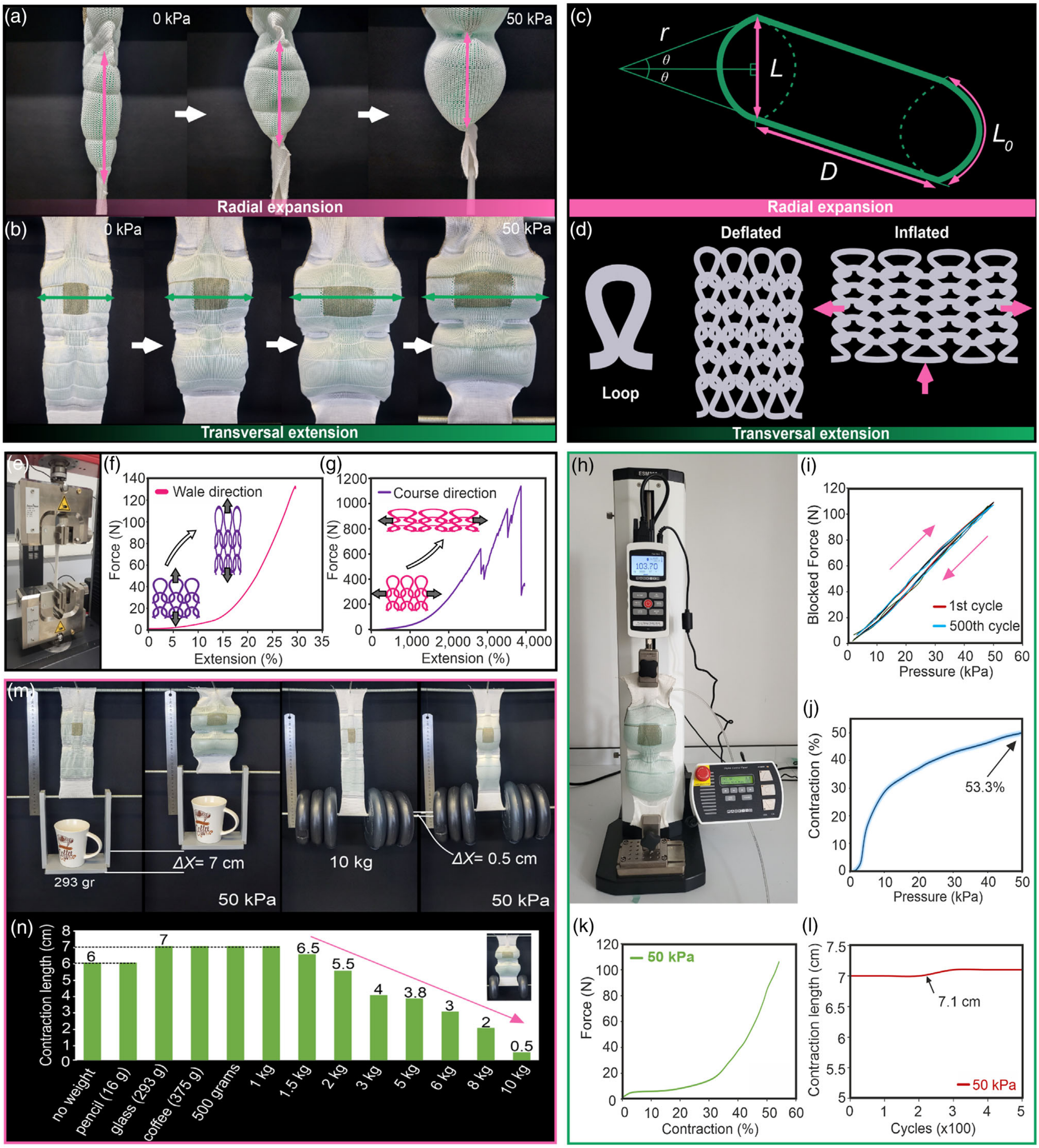

Figure 4. The contraction actuation mechanism of soft knitted pouch motor. a) Radial expansion of the pouch motor. As the air pressure increases, the radial expansion of the motor also increases. b) Effect of increasing air pressure on the transversal extension of the pouch motor. This deformation is based on the sliding of the knit loop structure in the weft direction. c) Theoretical model of the pouch motors. d) Loop structure of the knitted pouch motor in deflated and inflated states. e) Universal testing machine. f) Tensile test of Spectra knitted fabric sample in the wale direction. g) Tensile test of a Spectra knitted fabric sample in the course direction. h) Experimental setup. The pouch motor is connected to an air tube and pressure sensor. Here, displacement, force, and air pressure are recorded. i) Blocked force (N)–pressure (kPa) relationship during 500 cycles at pressures ranging from 0 to 50 kPa. j) Maximum % contraction at pressures in the range of 0–50 kPa. k) Force (N)–contraction (%) relationship at 50 kPa. l) Change in contraction length (cm) during 500 cycles. m) Showing that the 3D knitted sensing pouch motor exhibits the ability to lift up to 10 kg of weight under 50 kPa. n) Contraction length (cm) of the pouch motor under various weights at 50 kPa pressure.

performance. For this reason, we analyzed the structural integrity of Spectra base fabric of the pouch motor by subjecting it to uniaxial tensile testing using a mechanical testing machine (Figure 4e). The fabric sample exhibits a 32% extension at 138 N in the wale direction (Figure 4f) and 2800% extension at 620 N in the course direction (Figure 4g). After achieving a 2800% extension at 620 N, a decline in the graph was observed due to the loop breakage. Knitted structures are known for their construction, which involves interlocking loops of yarn in both the course and wale directions.[63] The interlocking loops in both directions distribute forces evenly, ensuring that the fabric can withstand the stresses associated with the contraction and extension cycles of the motor. From these perspectives, when additional weight is applied to the pouch motor, it tends to contract along the y-axis without significant extension, even at lower internal air pressure, making it easily deform in the transverse direction.

The knitted pouch motor was subjected to actuation tests as isotonic (constant load) and isometric (constant length). The measurements were performed under static conditions. Isometric tests were used to investigate the relationship between tensile force and pressure. The isometric tests consisted of each soft pouch motor being pretensioned to 0.5 N (chosen to minimize slack in embedded fibers while also reducing effects on actuator performance and pressurized to 50 kPa (chosen to avoid failure), as shown in Figure 4h. This was performed for three trials. The actuator can generate a maximum blocked force of 107 ± 2.2 N when pressurized up to the maximum operating pressure of 50 kPa (Figure 4i). Due to the limited pressure threshold of the air bladder, pressures exceeding 50 kPa were not applied. The hysteresis of the pouch motor, exposed to 500 cycles of inflation and deflation, is not significant. This decrease in hysteresis is attributed to the strategic placement of elastomeric yarns in the course direction. Experiments demonstrate that the output force of the pouch motor increases with input air pressures. Isotonic tests were used to investigate the maximum contraction with increasing pressure. Typical pneumatic contraction actuators can deliver a maximum contraction of around 25–35%, for example, McKibben muscle and other pouch motors.[14,64] Our pouch motor has exhibited a maximum contraction behavior of up to 53.3% with increasing pressure (Figure 4j).

Figure 4k shows the force–contractile relationship at a constant 50 kPa maximum pressure. The pouch motor exhibits a 53.3% contraction, corresponding to a reduction in length of 7 cm. After subjecting the pouch motor to 500 inflation and deflation cycles at 50 kPa, it was observed that its contraction increased to 7.1 cm after 235 cycles (Figure 4l). This demonstrates the remarkable durability of the pouch motor, as repeated inflation and deflation did not result in structural degradation. This data underscores resilience of the pouch motor and stability over multiple inflation and deflation cycles, making it a reliable component for various applications. The minimal change in its contraction behavior indicates its robust design and suitability for long-term use.

By first subjecting the pouch motor to rigorous mechanical testing, we gained insight into its baseline capabilities. However, it was also crucial to examine how it would perform under more realistic conditions that it might encounter in everyday use. The 50 kPa test was conducted to simulate the kinds of loads it could face in practical applications, allowing us to assess its functionality and reliability in scenarios that align with its intended use. The contraction length of the muscle structure was measured while loads varied from 125 g to 10 kg (Figure 4m,n and Figure S4, Supporting Information). There was a general trend for the contraction length of the muscle structure to be reduced as the load it carried was increased. At a pressure of 50 kPa, a maximum contraction of 7 cm has been measured. To ensure the pouch motor reaches its full length, it is necessary to apply a lightweight load, such as a 293 g (glass weight), as depicted in Figure 4m. Knitted structures shrink or curl after production (once removed from the knitting machine) due to unbalanced forces generated by the yarn loops. In their unstressed or relaxed state, knitted fabrics typically exhibit a non-fully stretched configuration. This phenomenon arises due to the inherent looped structure and the elastic nature of the constituent yarns. The inherent gathering observed in relaxed knitted fabrics stems from the ability of the yarn loops to adjust and move within the overall fabric structure. Therefore, applying tension is essential to counteract these tendencies and achieve full extension of the pouch motor. This tensioning process serves the purpose of mitigating the inherent gathering within the fabric. By doing so, it facilitates a more uniform alignment of the yarn loops. This tensioning technique aids in revealing the actual size and shape of the knitted pouch motors. As a result, this approach ensures that the pouch motor is not only theoretically sound but also practically viable.

4.2. Sensor Characterization

Soft capacitive pressure sensor of knitted pouch motors consists of conductive knitted layers to serve as electrode layers and thermoplastic polyurethane film dielectric layer, illustrated in **Figure 5**a. We employed an Ag-coated polyamide yarn to knit the conductive electrode surface. Figure 5b illustrates an optical microscopy image of the loops in the conductive knitted layer. The incorporation of a capacitance pressure sensor into a knitted pouch motor allows for the precise calculation of capacitance variations in direct reaction to changes in both the air pressure delivered to the pouch motor and contraction motion. This sensor integration provides real-time monitoring and feedback, offering valuable insights into the interplay between internal air pressure and pouch motor deformation and how it influences the behavior of the sensor.

To assess the electrical response of these sensors to applied air pressure, we designed an experimental setup for the synchronized collection of mechanical and electrical data, employing a mechanical tester and a capacitance meter. The capacitance of the sensor (C_{sensor}) can be understood through several parameters, including electrode area (A), dielectric thickness (d), the dielectric permittivity of a vacuum (ε_0), and the relative permittivity of the dielectric (ϵ_r). Equation (1) quantifies the changes in capacitance attributable to variations in dielectric layer thickness and electrode area.

$$C_{\text{sensor}} = \varepsilon_0 \varepsilon_r \frac{A}{d_0} \tag{12}$$

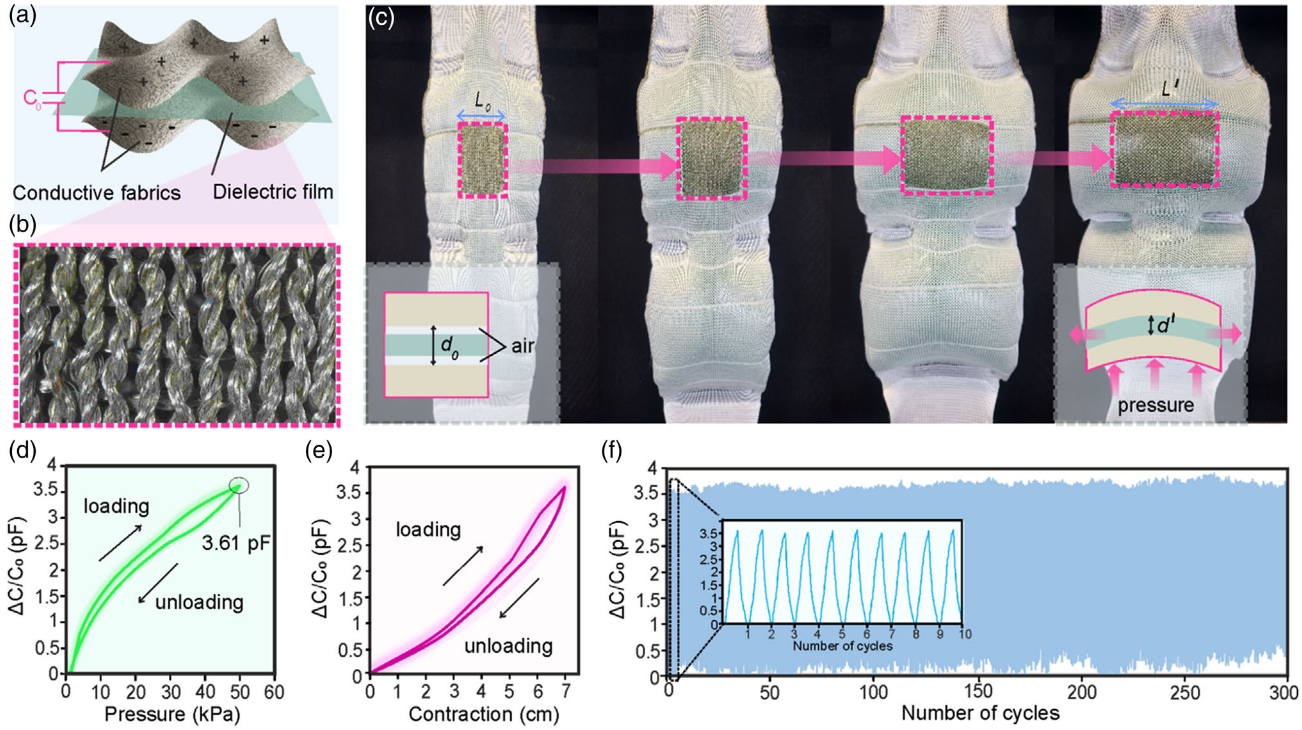

Figure 5. Capacitive pressure sensing of knitted pouch motor. a) Cross-sectional view of the capacitive sensor comprising conductive electrodes at the top and bottom, separated by a dielectric film. b) Optical microscopy image of the loop structured sensor electrode. c) Actual images of the sensor increasing air pressure. d) Relative change in capacitance during the loading/unloading process under 50 kPa. e) Relative capacitance change of sensor with increasing and decreasing contraction length (cm) of the pouch motor. f) Sensor repeatability test.

Pressure application causes the conductive knitted area to stretch, leading to an expansion in the surface of the electrode (Figure 5c). This stretching results in an increased capacitance of the electrode due to the larger surface area, enabling better overlap between the conductive layers. The width of the sensor exhibits a 100% increase when the pouch motor is inflated. When the fabric is in its unstrained state, the closely spaced knit loops of the sensor create numerous conduction paths, resulting in a low initial resistance. As the fabric undergoes stretching, the morphology of the loop changes, primarily due to yarn slipping at the interlooping points. This change reduces the contact areas between the knitting loops, thereby improving the contact resistance ($R_{contact}$). As $R_{contact}$ increases, the capacitance of the sensor also increases because of the expanded surface area of the electrode caused by stretching. Consequently, the connections between the arc segments of the knitting loops recede, leading to visible gaps and open circuits, which further raise the resistance of the knit sensors. Besides, as the pouch motor receives internal air pressure, the air gaps between the conductive layers and the dielectric film gradually close. This process leads to an increase in capacitance, enhancing the sensitivity of the sensor. The decrease in air gaps acts like a secondary dielectric layer, leading to a more noticeable change in capacitance when the sensor experiences mechanical deformation or changes in pressure.

In Figure 5d, we observe the electrical response of the sensor under applied pressure levels, ranging from increasing to decreasing, up to 50 kPa. Notably, the change in capacitance is most pronounced when subjected to the maximum pressure. The sensitivity (S) of the pressure sensor can be calculated as $S = \Delta C/C_0/P$, where P represents the applied pressure and ΔC and C_0 signify the change in capacitance and baseline capacitance, respectively. The pressure sensitivity of the sensor is determined to be $722 \times 10^{-4}\,\text{kPa}^{-1}$. The relationship between the output electric signals (normalized capacitance change, $\Delta C/C_0$) and the contraction is depicted in Figure 5e and Movie S4, Supporting Information. The relative capacitance increased in pouch motors that contract with increasing pressure. In the pressure unloading phase, the relaxation of stress within the material leads to a partial recovery of its original configuration. However, deformations and hysteresis persist, especially within the pressure range between 50 and 30 kPa, and as the contraction decreases. Below 30 kPa, the decreasing hysteresis indicates a notable transition, potentially corresponding to the saturation of deformations or the establishment of a quasiequilibrium state within the material. As a result, the influence of pressure variations on the capacitive sensor becomes less pronounced, leading to reduced hysteresis. Overall, the observed hysteresis behavior reflects the intricate interplay between material properties, structural dynamics, and sensor characteristics in the textile-knitted pouch-based pressure sensing system.

To evaluate the stability of the pressure sensors concerning pressure sensitivity, we conducted a repeated loading/unloading cyclic test, as shown in Figure 5f. The sensor demonstrated both long-cycle stability and satisfactory robustness after 300 loading and unloading cycles at 50 kPa of air pressure.

These results signify that the soft pressure sensor is well suited for detecting air pressure levels during the contraction process and holds promise for applications requiring robotic control. The stable and reproducible signal affirms the potential of the sensor for long-term usage. Therefore, the designed pressure sensor meets the requirements for effectively monitoring actuation and contractions in the realm of soft robotics.

5. Application Demonstration

The high contraction ratio and high output force exhibited by pouch motors make them an ideal choice for incorporation into soft artificial muscle robots. In our study, we have selected to demonstrate exercise and walking application of pouch motors in the context of an exoskeleton robot designed to address foot drop syndrome. In this robotic design, as depicted in **Figure 6**a, the system featured an electropneumatic control unit (Figure 6a(i)) that could be comfortably secured around the waist, conductive wires transmitting signals from the heel to the pneumatic control system (Figure 6a(ii)), pressure-sensing socks, and our pouch motor easily attachable to the foot and ankle (Figure 6a(iii)). Within the control system worn around the waist, there is a pneumatic pump, a battery, and an Arduino Uno microcontroller board. These components collectively contribute to the functionality and operation of the system.

Healthy individuals naturally perform the "heel strike," "stance," "heel off," and "swing" walking phases while walking (Figure 6b).[65] These phases involve generating an ankle dorsiflexion moment in the swing phase of each limb to lift the foot and facilitate ground clearance. However, when it comes to exoskeletons, concerns such as rigidity, high development costs, portability, alignment complications with the biological joint they are trying to assist, and comfort over extended periods of use

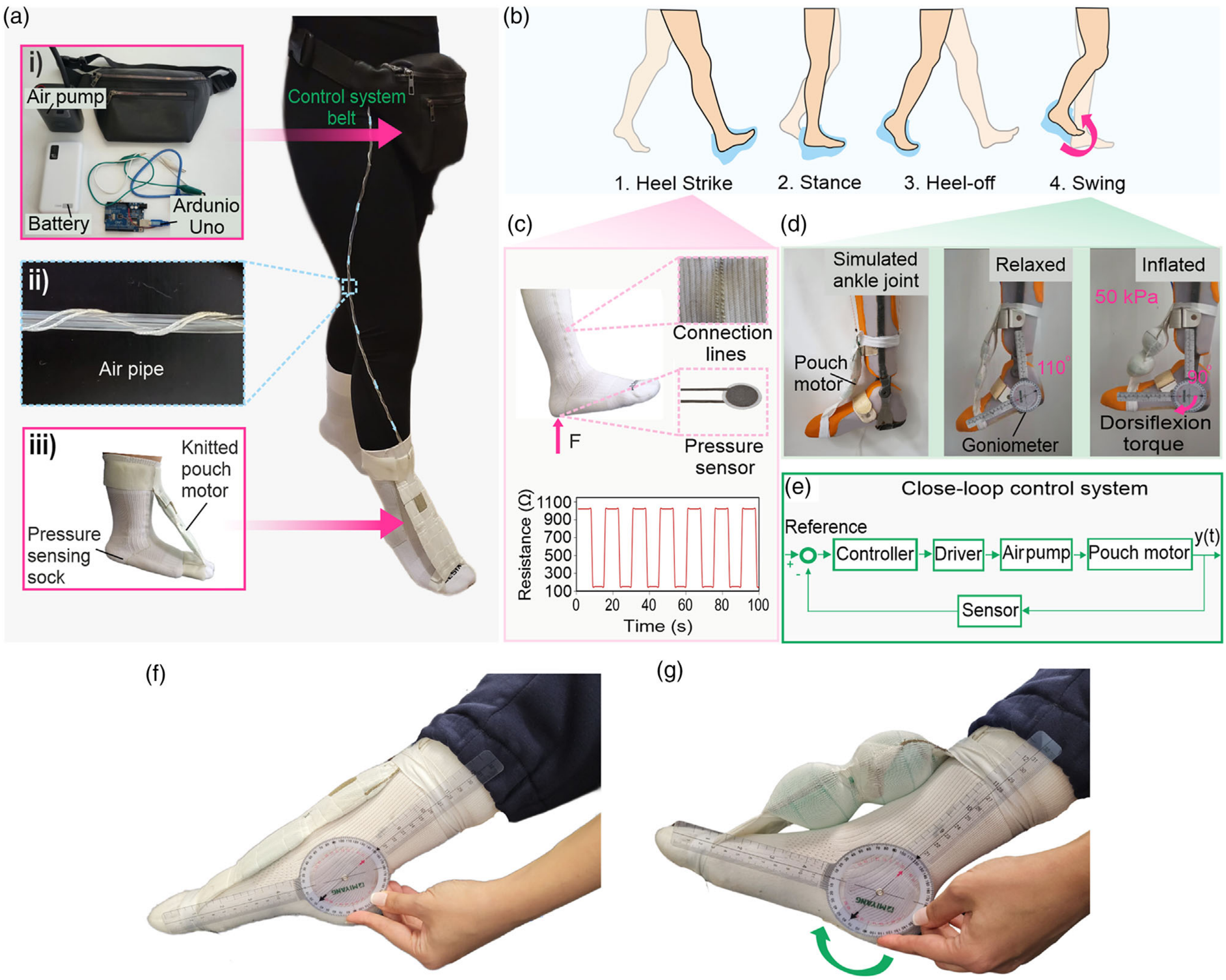

Figure 6. Application demonstration of the soft pouch motor in assistive robotics. a) Showing the concept behind the soft ankle-foot orthosis exosuit. b) Phases of the human gait. c) Functionality and application of the textile-based resistive pressure sensing sock. d) Dorsiflexion motion of the simulated ankle joint by soft pouch motor. e) Close-loop control block diagram. f) Deflated pouch motor fastened to a human foot. g) Dorsiflexion of the human foot using pouch motors that is inflated.

arise.[66] By using our soft pouch motor, developed through knitting technology, we introduce valuable addition to the field of assistive artificial muscle devices. Its adaptability, convenience, lightweight nature, cost-effectiveness, and comfort in both robot and human interactions make it a good fit for wearable applications, enabling prolonged daily usage.

The soft pouch motor securely attaches to the foot and ankle using textile straps to generate torque for lifting the simulated ankle joint. Our assistive wearable device consists of a textile-based resistive pressure sensor[67] (Figure S5, Supporting Information) designed to be placed on the heel of the sock and a soft pouch motor. The soft pouch motor is controlled with a single resistive pressure sensor, specifically a heel contact sensor, which detects gait timing. As the swing walking phase initiates, the ankle dorsiflexes, raising the toes to clear the ground for the upcoming gait cycle that begins at the heel strike.[68] The input received from the heel activates the pneumatic system of the actuator, causing it to expand and subsequently inducing a contraction motion, resulting in dorsiflexion of the foot. Dorsiflexion involves an increase in the joint angle and an upward movement of the toes. The presence–absence resistive sensor placed on the heel of the sock is connected using thermoplastic-coated conductive threads for both positive and negative connections (Figure 6c). As a result, the soft pouch motor automatically adapts to changes in the gait speed of the wearer, as the pressure sensor detects when the heel is on the ground and pressure should be applied to the pouch motor. Tests have indicated that the pouch motor has the potential to provide dorsiflexion assistance, as evidenced by the simulated ankle achieving a dorsiflexion torque of 20° at 50 kPa air pressure, as shown in Figure 6d and Movie S5, Supporting Information. This indicates the potential effectiveness of the motor in supporting ankle dorsiflexion. The response time is ≈1 s. Optimizing the equipment constituting the pneumatic control system has the potential to further reduce response time. Proper design, sizing, and configuration of valves, pressure regulators, pipes, and powerful pumps in pneumatic systems are crucial for achieving faster response times. In the future, by focusing on the design and engineering of the pneumatic system, we will achieve even faster response times of the pouch motors.

The schematic diagram of the closed-loop control system illustrating the operational principle of our soft robotic system is presented in Figure 6e. After evaluating the dorsiflexion torque capability on the simulated ankle joint, the ability of the pouch motor to apply torque on the human foot was also tested. Figure 6f indicates the deflated pouch motor securely attached to a human foot, showcasing its initial state. The dorsiflexion of the human foot is demonstrated through the inflated pouch motor, as shown in Figure 6g. It successfully applies ≈35° of dorsiflexion torque to the human foot at 50 kPa pressure. This depiction highlights the dynamic functionality of the pouch motor in facilitating dorsiflexion, underlining its potential as a valuable component for supporting walking and foot drop exercises. Movie S6, Supporting Information, has been recorded that shows exercise and walking motions on a healthy human foot.

The pouch motor is anchored at the ankle and foot, ensuring the inflation region—the part that transversal extension and radial expansion—does not touch the foot itself, as shown in Figure S3, Supporting Information. This targeted inflation focuses solely on lifting the foot, minimizing any potential contact-induced discomfort. The device utilizes a securing element (strap, band, or Velcro) that allows users to adjust the tightness around the ankle and toes (Figure S6, Supporting Information). This personalization feature ensures a comfortable and secure fit, preventing the pouch motor from slipping or causing irritation due to excessive tightness. In simpler terms, this soft pouch foot lift assist is designed to be gentle on your foot. It inflates only where needed for lifting, and the pressure and tightness can be adjusted for your comfort. Furthermore, in general, the duration of the dorsiflexion phase in a walking cycle covers a short period. Therefore, there will be no comfort issues associated with it.

6. Discussion

In **Table 2**, we compare the performance metrics of existing pneumatic pouch motors studies with knitted pouch motors,

Table 2. Comparison of pneumatic pouch motors.

Work	Material	Max. contraction ratio [%]	Max. force [N]	Pressure [kPa]	Sensor type and sensor sensitivity
Pouch[14]	Film	28	100	40	–
Flat film PAM[76]	Film	44	300	30	Capacitive sensor[a)] (not embed)
Origami pouch[13]	Film	40.6 (series) 55.9 (parallel)	175.2	30	–
Flat fabric PAM[22]	TPU-coated woven commercial fabric	23.84	118	172	Capacitive sensor[a)] (not embed)
Paired pouch[16]	TPU-coated woven commercial fabric	41.9	100	90	–
Gusseted pouch[15]	TPU-coated woven commercial fabric	42.6	100	40	–
CRAM[77]	TPU-coated woven commercial fabric	48.3	33.1	100	Capacitive sensor[a)] (not embed)
X-PAMs[78]	TPU-coated woven commercial fabric	0.92	134.7	150	–
Knitted sensing pouch motors (This work)	Knitted fabric	0.53	107	50	Embedded capacitive sensor 722×10^{-4} kPa^{-1}

[a)]These data are not found in the article.

focusing on parameters such as contraction, force, pressure, and sensor sensitivity. However, it is essential to note that our primary objective is not to assert the superiority of our pouch motors over existing works in terms of specific performance metrics. Instead, the novelty of our work lies in demonstrating the utilization of textile computerized knitting technology for the design and fabrication of sensing fabric pouch motors. By employing textile knitting technology, we aim to enable rapid and scalable manufacturing of these motors. While our knitted pouch motors may exhibit similar average values for contraction, force, and pressure compared to those using film and TPU-coated materials, it is crucial to consider the longevity and durability factors. The utilization of film and TPU-coated materials in other studies may restrict their durability and render them less resilient in real-world applications. Our soft knitted pouch motor, integrating high-performance Spectra base yarn, effectively leverages its outstanding features, including cutting resistance and high strength. These attribute contributes to the overall durability and reliability of knitted pouch motors, making them suitable for practical artificial muscle applications.

7. Conclusion

Our muscle-inspired study has utilized 3D textile knitting technology to digitally fabricate soft and robust pouch motors, incorporating pneumatic-driven contraction motion programmed within their knit loop architecture. The soft pouch motor we have developed addresses the challenges of scalability and mass production while also positioning itself as a promising solution in the field of soft robotic artificial muscles. Our soft knitted pouch motor, integrating high-performance Spectra yarn, effectively leverages its outstanding features, including remarkable cutting resistance, lightweight design, and high strength, which set it apart from other film-based and woven fabric-based pouch motors. It displayed a high contraction ratio under 50 kPa pressure, with a maximum lifting capability of 10 kg a remarkable 53.3% contraction along the y-axis, and a transverse extension of 41.18% along the x-axis.

One noteworthy advantage of this compact design is the transverse extensibility provided by the knitting technology, resulting in a significantly improved contraction rate when compared to conventional woven fabric and film-based pouch motors. This enhanced performance has broad implications for various applications. Furthermore, the transverse extensibility has increased the area of the embedded capacitive sensor, leading to an enhanced capacitance change in pouch motor sensing technology.

The primary function of the motor is to offer dorsiflexion support, with the potential to address foot drop symptoms, although further empirical validation is needed. Furthermore, our research underscores its potential to drive advancements in powered orthoses. The inherent compliance and flexibility of the design facilitate the development of soft robotic devices that closely mimic the natural form and movement of the human body.

The pouch motor offers practical benefits, including enhanced user mobility, making it suitable for daily use and easy to put on. It is expected that forthcoming human subject trials will provide concrete evidence of these advantages. In this context, the work makes a valuable contribution to the field of soft robotic artificial muscle technologies. Furthermore, knitted pouch motors embedded within a wearable device or clothing during social touch and interactions can help people feel more connected to each other, whether in person or on digital platforms. Additionally, in the world of VR gaming, pouch motors can contribute to a heightened sense of touch and feedback. They can simulate the feel of virtual objects and environments, adding depth and realism to the gameplay. With their potential to provide lifelike sensations, knitted pouch motors can have the power to revolutionize the gaming experience, bringing players closer to their virtual worlds. The integration of pouch motors in haptic applications can offer exciting possibilities for enhancing the way we interact with digital environments and each other.

8. Experimental Section

Materials: Three types of yarns were used to manufacture the pouch motor sample. The ground structure was created using commercially available 435 dtex ultrahigh molecular weight polyethylene fiber (Polat Job Security Industry and Trade Co. Ltd., Bursa, Türkiye) and commercial 140/70 × 2 denier nylon-covered spandex yarn (Çombaş Industry and Trade Co. Ltd., İstanbul, Türkiye). The sensing structure of the actuator was built using a commercial 235 f/36 dtex 2-ply HC + B silver-plated nylon conductive yarn (Shieldex, Bremen, Germany). The linear resistance of this conductive yarn was 100 Ω m^{-1}, the elasticity was up to 17 500 m kg^{-1}, the tensile strength was 46 cN tex^{-1}, and the stretching was up to 15%. To make an air bladder, an impulse sealer machine (PCS 300, Brother, Nagoya, Japan), thermoplastic polyurethane film (Stretchlon 200, Fiber Glast, Brookville, OH, USA), and a polyurethane tube were used.

Fabrication: The sensing pouch motor sample was manufactured using 14 gauge v-bed weft knitting technology (Shima Seiki NSVR 122, Sakata Wakayama, Japan). It is composed of two rectangular-shaped pouches that are connected to each other. The pouch dimensions were 9 cm in width and 8 cm in height. The contraction line connecting the two pouches is located at the right and left edges of the pouch motor, measuring 1 cm in length and 3 cm in width. There is a central channel between the pouches that allow for the airflow of the air bladder. The pouch motor and electrodes of the sensor structures exhibited course density of 9 courses per inch and wale density of 9 wales per inch, resulting in a stitch density of 81 stitches per square inch. To secure the soft pouch motor to the foot and ankle with Velcro straps passing through, a seamless strap region has been created within the knit structure of the soft pouch motor (Figure S6, Supporting Information). To create two pouch air bladders, an impulse sealer machine (PCS 300, Brother, Nagoya, Japan), thermoplastic polyurethane film, and polyurethane tube were used. Pouch-shaped films were layered on top of one another, as shown in Figure 1(iv), and an impulse sealer was used to create a bond between them at a time setting of 5.5 s. A polyurethane tube was inserted into the open end, and a pneumatic system was used to inflate it.

Mechanical and Electrical Characterizations: The mechanical properties of yarn were tested using yarn grippers at a speed of 250 mm min^{-1} with a commercial uniaxial testing machine (Titan 5, James Heal, UK). The knitted samples prepared for modeling and simulation, according to their course and wale orientations, were subjected to mechanical testing using a 5 kN load cell on a uniaxial tensile testing machine (Zwick Roell Z005, Ulm, Germany) at a speed of 100 mm min^{-1}. Five 20 × 5 cm pieces of knit fabric were manufactured in the course-wale directions. Before testing, the samples were conditioned in a standard atmospheric environment for 24 h. The extension (mm) and force (N) values were recorded during the tests. The digital microscope was utilized to observe the morphological structure of the yarns.

The static and dynamic experimental characterization of the pouch motors was performed utilizing a motorized horizontal single-axis test stand (ESM 303, Mark-10, Copiague, NY, USA), which was equipped with a single-axis load cell, a pressure regulator, vacuum pump, pressure sensor, linear encoder, a custom amplifier circuit, and a specially designed program for collecting experimental data. One end of the actuator was fixed in a stationary position, while the other end was attached to a weak spring and a magnetic linear encoder. This setup allowed the actuator to easily perform a contraction motion when pressurized air was supplied to it, with the amount of contraction length being transferred to the computer as data based on the movement of the magnetic linear encoder. The capacitance value was measured using a capacitive touch sensor (MPR121 Proximity Capacitive Touch Sensor Controller, NXP, Eindhoven, The Netherlands). Experiments have been conducted in normal atmospheric conditions.

Actuation: Pressurized air was supplied by an air compressor (DN200/8/6, Stanley, Italy) connected to the actuator through a pressure regulator (VPPM, Festo, Germany) and two solenoid valves (2W-025-08, Senya, China), which were used to regulate the pressure level and inflate and deflate the actuator. The air pump and solenoid valve were controlled by the 5 V, 4-channel relay board and Arduino Uno microcontroller. Using an air pressure sensor (MPXHZ6250A, Freescale Semiconductor, USA), the internal pressure of the actuator was measured.

Close-Loop Control System: A microcontroller (Arduino Uno Atmega328P, Microchip, USA) as the control unit, a 10 W power bank as the power source of the control unit, and a portable air compressor (Model 8010A, California Air Tools, USA) as the actuator were used to provide a pneumatic actuation source. The pressure-sensing sock was used for sensor feedback from the control system. The pressure-measuring sock can take on two values: short circuit and open circuit. If the measured resistance value is 120, it means the sensor is in a short-circuit state, and if it is 1023, it means it is in an open-circuit state. When the sensor is in a short-circuit state, it means that pressure is applied to the ball of the foot touching the ground. When it is in an open-circuit state, it means that no pressure is being applied. When the sensor is in a short-circuit state, the controller sends a signal for the air compressor to start working, and when it is in an open-circuit state, the air compressor stops due to high pressure.

Supporting Information

Supporting Information is available from the Wiley Online Library or from the author.

Acknowledgements

This work was supported by the Horizon Europe European Research Council (ERC) project "Textile-Based Wearable Soft Robotics with Integrated Sensing, Actuating, and Self-Powering Properties—TEXWEAROTS" (project no. 101042402) and the Scientific and Technological Research Council of Türkiye (TUBITAK), project "Development of Textile-Based Robotics for Drop Foot Syndrome" (grant no. 120C118). The authors also acknowledge the members of the Soft Sensors Lab for their support. The authors would like to thank Polat Job Security Industry and Trade Company, Bursa, Türkiye for supplying the yarns used in the study. The authors are grateful to Yüksel ÜNGÖR from Tetaş for technical support on the Shima Seiki weft knitting machine.

Conflict of Interest

The authors declare no conflict of interest.

Author Contributions

A.F.Y., A.T.A., and O.A. conceived the idea. A.F.Y. designed and fabricated samples, performed the experiments, analyzed the data, designed figures and videos, and wrote the paper. K.O. and M.F.C. designed mechanical characterization test rig. K.O. did the coding for data collection and created the pneumatic system. M.F.C. manufactured components for a mechanical characterization test rig and designed close-loop control system. B.T. performed modeling and finite element analysis. O.A. revised the manuscript and obtained funding. A.T.A., G.I., and O.A. supervised this project.

Data Availability Statement

The data that support the findings of this study are available from the corresponding author upon reasonable request.

Keywords

capacitive sensors, pneumatic artificial muscles, pouch motors, soft robotics, soft sensors, textile robotics, wearable robots

Received: December 20, 2023
Revised: May 6, 2024
Published online: June 2, 2024

[1] W. R. Frontera, J. Ochala, *Calcif. Tissue Int.* **2015**, *96*, 183.
[2] K. Groeneveld, *Acta Physiol.* **2022**, *234*, e13791.
[3] A. A. Biewener, *J. Exp. Biol.* **2016**, *219*, 285.
[4] G. Iolascon, M. Paoletta, S. Liguori, C. Curci, A. Moretti, *Front. Endocrinol.* **2019**, *10*, 794.
[5] S. Cohen, J. A. Nathan, A. L. Goldberg, *Nat. Rev. Drug Discovery* **2015**, *14*, 58.
[6] D. Yang, M. Feng, G. Gu, *Adv. Mater.* **2024**, *36*, 2306928.
[7] M. Pan, C. Yuan, X. Liang, T. Dong, T. Liu, J. Zhang, J. Zou, H. Yang, C. Bowen, *Adv. Intell. Syst.* **2022**, *4*, 2100140.
[8] A. F. Yilmaz, F. Khalilbayli, K. Ozlem, H. M. Elmoughni, F. Kalaoglu, A. T. Atalay, G. Ince, O. Atalay, *Biomimetics* **2022**, *7*, 249.
[9] C. Thalman, P. Artemiadis, *Wearable Technol.* **2020**, *1*, e3.
[10] M. Cianchetti, C. Laschi, A. Menciassi, P. Dario, *Nat. Rev. Mater.* **2018**, *3*, 143.
[11] P. Polygerinos, N. Correll, S. A. Morin, B. Mosadegh, C. D. Onal, K. Petersen, M. Cianchetti, M. T. Tolley, R. F. Shepherd, *Adv. Eng. Mater.* **2017**, *19*, 1700016.
[12] T. Hiraki, K. Nakahara, K. Narumi, R. Niiyama, N. Kida, N. Takamura, H. Okamoto, Y. Kawahara, *IEEE Robot. Autom. Lett.* **2020**, *5*, 4180.
[13] S. Li, J. Lin, H. Kang, Y. Cheng, Y. Chen, *Robot. Auton. Syst.* **2022**, *149*, 103983.
[14] R. Niiyama, X. Sun, C. Sung, B. An, D. Rus, S. Kim, *Soft Robot.* **2015**, *2*, 59.
[15] J. H. Jang, B. Jamil, Y. Moon, A. Coutinho, G. Park, H. Rodrigue, *IEEE/ASME Trans. Mechatron.* **2023**, *28*, 3053.
[16] N. Oh, Y. J. Park, S. Lee, H. Lee, H. Rodrigue, *Adv. Mater. Technol.* **2019**, *4*, 1800414.
[17] H. L. Sweeney, D. W. Hammers, *Cold Spring Harb. Perspect. Biol.* **2018**, *10*, a023200.
[18] W. Herzog, G. Schappacher-Tilp, *J. Biomech.* **2023**, *155*, 111659.
[19] V. Oguntosin, A. Akindele, *Sens. Actuators, A* **2019**, *297*, 111523.
[20] S. M. Mirvakili, I. W. Hunter, *Adv. Mater.* **2018**, *30*, 1704407.
[21] E. J. Ball, M. A. Meller, J. B. Chipka, E. Garcia, *Smart Mater. Struct.* **2016**, *25*, 115024.

[22] W. Kim, H. Park, J. Kim, *IEEE Robot. Autom. Lett.* **2021**, *6*, 2603.
[23] H. Lee, N. Oh, H. Rodrigue, *IEEE Robot. Autom. Mag.* **2020**, *27*, 65.
[24] J. Wirekoh, L. Valle, N. Pol, Y. L. Park, *Soft Robot.* **2019**, *6*, 768.
[25] Z. Yoder, N. Kellaris, C. C. Markopoulou, D. Ricken, S. K. Mitchell, M. B. Emmett, R. F. Weir, J. Segil, C. Keplinger, *Front. Robot.* **2020**, *7*, 586216.
[26] V. Sanchez, C. J. Payne, D. J. Preston, J. T. Alvarez, J. C. Weaver, A. T. Atalay, M. Boyvat, D. M. Vogt, R. J. Wood, G. M. Whitesides, C. J. Walsh, *Adv. Mater. Technol.* **2020**, *5*, 2000383.
[27] R. Zakeri, R. Zakeri, *Sci. Rep.* **2022**, *12*, 3627.
[28] N. Kellaris, V. G. Venkata, G. M. Smith, S. K. Mitchell, C. Keplinger, *Sci. Robot.* **2018**, *3*, eaar3276.
[29] L. Tynan, G. Naik, G. D. Gargiulo, U. Gunawardana, *Actuators* **2021**, *10*, 38.
[30] X. Tang, H. Li, T. Ma, Y. Yang, J. Luo, H. Wang, P. Jiang, *Actuators* **2022**, *11*, 331.
[31] P. H. Nguyen, W. Zhang, *Sci. Rep.* **2020**, *10*, 9638.
[32] J. Pu, K. Ma, Y. Luo, S. Tang, T. Liu, J. Liu, M. Leung, J. Yang, R. Hui, Y. Xiong, X. Tao, *Int. J. Extrem. Manuf.* **2023**, *5*, 042007.
[33] N. D. Naclerio, E. W. Hawkes, *IEEE Robot. Autom. Lett.* **2020**, *5*, 3406.
[34] H. K. Yap, F. Sebastian, C. Wiedeman, C. H. Yeow, in *IEEE Int. Conf. on Rehabilitation Robotics*, London, UK **2017**.
[35] P. H. Nguyen, F. Lopez-Arellano, W. Zhang, P. Polygerinos, in *IEEE Int. Conf. on Intelligent Robots and Systems*, Macau, China **2019**.
[36] C. T. O'Neill, C. M. McCann, C. J. Hohimer, K. Bertoldi, C. J. Walsh. *Soft Robot.* **2022**, *9*, 163.
[37] B. Seyidoğlu, A. Rafsanjani, *Device* **2024**, *2*, 100226.
[38] H. K. Yap, P. M. Khin, T. H. Koh, Y. Sun, X. Liang, J. H. Lim, C. H. Yeow. *IEEE Robot. Autom. Lett.* **2017**, *2*, 1383.
[39] P. H. Nguyen, I. B. Imran Mohd, C. Sparks, F. L. Arellano, W. Zhang, P. Polygerinos, in *IEEE Int. Conf. on Robotics and Automation*, Montreal, QC, Canada **2019**.
[40] X. Liang, H. Cheong, Y. Sun, J. Guo, C. K. Chui, C.-H. Yeow, *IEEE Robot. Autom. Lett.* **2018**, *3*, 2702.
[41] J. M. Dávila-Vilchis, J. C. Ávila-Vilchis, A. H. Vilchis-González, L. A. Zúñiga-Avilés, J. M. Jacinto-Villegas, *Machines* **2022**, *10*, 871.
[42] J. Ma, D. Chen, Z. Liu, J. Wei, X. Zhang, Z. Zeng, Y. Jiang, *J. Bionic Eng.* **2023**, *20*, 2661.
[43] H. Wang, D. Weerasinghe, D. Mohotti, P. J. Hazell, *Int. J. Mech. Sci.* **2021**, *204*, 106574.
[44] H. M. Elmoughni, A. F. Yilmaz, K. Ozlem, F. Khalilbayli, L. Cappello, A. T. Atalay, G. Ince, O. Atalay, *Actuators* **2021**, *10*, 94.
[45] A. P. Gerratt, H. O. Michaud, S. P. Lacour, *Adv. Funct. Mater.* **2015**, *25*, 2287.
[46] S. Gong, W. Schwalb, Y. Wang, Y. Chen, Y. Tang, J. Si, B. Shirinzadeh, W. Cheng, *Nat. Commun.* **2014**, *5*, 3132.
[47] L. Viry, A. Levi, M. Totaro, A. Mondini, V. Mattoli, B. Mazzolai, L. Beccai, *Adv. Mater.* **2014**, *26*, 2659.
[48] C. Gumus, K. Ozlem, F. Khalilbayli, O. F. Erzurumluoglu, G. Ince, O. Atalay, A. T. Atalay, *Micro Nano Eng.* **2022**, *15*, 100140.
[49] A. Pazar, F. Khalilbayli, K. Ozlem, A. F. Yilmaz, in *Int. Computer Science and Engineering Conf.*, Diyarbakir, Türkiye **2022**.
[50] A. F. Yilmaz, I. A. K. Ahmed, C. Gumus, K. Ozlem, M. S. Cetin, A. T. Atalay, G. Ince, O. Atalay, *Adv. Sensor Res.* **2023**, *3*, 2300121.
[51] M. G. Mohammed, R. Kramer, *Adv. Mater.* **2017**, *29*, 1604965.
[52] L. Qiu, M. B. Coskun, Y. Tang, J. Z. Liu, T. Alan, J. Ding, V. T. Truong, D. Li, *Adv. Mater.* **2016**, *28*, 194.
[53] L. Q. Tao, K. N. Zhang, H. Tian, Y. Liu, D. Y. Wang, Y. Q. Chen, Y. Yang, T. L. Ren, *ACS Nano* **2017**, *11*, 8790.
[54] Y. L. Park, C. Majidi, R. Kramer, P. Bérard, R. J. Wood, *J. Micromech. Microeng.* **2010**, *20*, 125029.
[55] C. Dagdeviren, P. Joe, O. L. Tuzman, K. Park, K. J. Lee, Y. Shi, Y. Huang, J. A. Rogers, *Extreme Mech. Lett.* **2016**, *9*, 269.
[56] C. Dagdeviren, B. D. Yang, Y. Su, P. L. Tran, P. Joe, E. Anderson, J. Xia, V. Doraiswamy, B. Dehdashti, X. Feng, B. Lu, R. Poston, Z. Khalpey, R. Ghaffari, Y. Huang, M. J. Slepian, J. A. Rogers, *Nat. Mater.* **2015**, *14*, 728.
[57] M. Amjadi, K. U. Kyung, I. Park, M. Sitti, *Adv. Funct. Mater.* **2016**, *26*, 1678.
[58] A. Chortos, Z. Bao, *Mater. Today* **2014**, *17*, 321.
[59] O. Atalay, A. T. Atalay, J. Gafford, C. Walsh, *Adv. Mater. Technol.* **2018**, *3*, 1700237.
[60] G. Agarwal, N. Besuchet, B. Audergon, J. Paik, *Sci. Rep.* **2016**, *6*, 34224.
[61] P. Moseley, J. M. Florez, H. A. Sonar, G. Agarwal, W. Curtin, J. Paik, *Adv. Eng. Mater.* **2016**, *18*, 978.
[62] F. Connolly, D. A. Wagner, C. J. Walsh, K. Bertoldi, *Extreme Mech. Lett.* **2019**, *27*, 52.
[63] R. H. Gong, in *Specialist Yarn and Fabric Structures: Developments and Applications* Woodhead Publishing, UK **2011**.
[64] F. Daerden, D. Lefeber, *Eur. J. Mech. Environ. Eng.* **2002**, *47*, 11.
[65] L. N. Awad, A. Esquenazi, G. E. Francisco, K. J. Nolan, A. J. Jayaraman, *NeuroEng. Rehabil.* **2020**, *17*, 80.
[66] C. M. Thalman, Q. P. Lam, P. H. Nguyen, S. Sridar, P. Polygerinos, in *IEEE Int. Conf. on Intelligent Robots and Systems (IROS)*, Madrid, Spain **2018**.
[67] O. Atalay, *J. Text. Eng.* **2018**, *25*, 140.
[68] J. Perry, J. M. Burnfield, *J. Sports Sci. Med.* **2010**, *9*, 353.
[69] C. M. Thalman, J. Hsu, L. Snyder, P. Polygerinos, in *IEEE Int. Conf. on Robotics*, Montreal, Canada **2019**.
[70] C. M. Thalman, T. Hertzell, H. Lee, in *IEEE Int. Conf. on Soft Robotics*, New Haven, CT **2020**.
[71] H. D. Yang, B. T. Greczek, A. T. Asbeck. *Front. Robot. AI* **2019**, *5*, 136.
[72] M. Schara, M. Zeng, B. Jumet, D. J. Preston, *Front. Robot. AI* **2022**, *14*, 1012862.
[73] M. Yang, J. Wu, W. Jiang, X. Hu, M. I. Iqbal, F. Sun, *Adv. Funct. Mater.* **2023**, *33*, 2210351.
[74] Y. Luo, K. Wu, A. Spielberg, M. Foshey, D. Rus, T. Palacios, W. Matusik, in *Proc. CHI Conf. on Human Factors in Computing Systems*, ACM, New York, NY **2022**.
[75] V. Sanchez, K. Mahadevan, G. Ohlson, M. A. Graule, M. C. Yuen, C. B. Teeple, J. C. Weaver, J. McCann, K. Bertoldi, R. J. Wood. *Adv. Funct. Mater.* **2023**, *33*, 2212541.
[76] J. Kwon, S. J. Yoon, Y. Park, *IEEE Trans. Robot.* **2020**, *36*, 743.
[77] D. Xie, J. Liu, S. Zuo. *IEEE Robot. Autom. Lett.* **2021**, *6*, 8599.
[78] M. Feng, D. Yang, L. Ren, G. Wei, G. Gu, *Sci. Adv.* **2023**, *9*, eadi7133.